

The effect of oxo-component on the high-pressure behavior of amphiboles

P. COMODI,¹ T. BOFFA BALLARAN,² P.F. ZANAZZI,^{1,*} C. CAPALBO,¹ A. ZANETTI,³ AND S. NAZZARENI¹

¹Dipartimento di Scienze della Terra, Università di Perugia, 06100 Perugia, Italy

²Bayerisches Geoinstitut, Universität Bayreuth, D-95440 Bayreuth, Germany

³CNR—Istituto di Geoscienze e Georisorse, 27100 Pavia, Italy

ABSTRACT

The role of the oxo-component on the compressibility of amphibole was studied by means of high-pressure in situ single-crystal X-ray diffraction on two natural kaersutite megacrysts (samples DL5 and FR12) from alkaline basalts. The oxo-component varies significantly (1.1 and 1.9 apfu in DL5 and FR12, respectively), whereas the cation composition is very similar, apart from the $\text{Fe}^{3+}/(\text{Fe}^{2+}+\text{Fe}^{3+})$, which is 0.33 in DL5 and ~ 1 in FR12. The larger oxo-component of FR12 is attributed to the $\text{Fe}^{2+} + \text{OH}^- = \text{Fe}^{3+} + \text{O}^{2-} + \frac{1}{2}\text{H}_2$ substitution.

Unit-cell parameters were collected at different pressures up to about 8 GPa. Structural refinements of both samples were performed with data collected at different P up to 6 GPa. Fitting the P - V data to a third-order Birch Murnaghan EoS yielded the following parameters: $K_0 = 94(1)$ GPa, $K' = 6.3(4)$, and $V_0 = 903.6(2)$ Å³ for FR12 and $K_0 = 91(2)$ GPa, $K' = 6.2(4)$, and $V_0 = 914.1(2)$ Å³ for DL5. The axial moduli of the two amphibole samples were: $K_{0a} = 86(3)$ GPa, $K'_a = 7(1)$, and $a_0 = 9.815(2)$ Å; $K_{0b} = 115(3)$ GPa, $K'_b = 4.8(8)$, and $b_0 = 18.012(2)$ Å; $K_{0c} = 112(5)$ GPa, $K'_c = 7(1)$, and $c_0 = 5.300(1)$ Å for sample FR12 and $K_{0a} = 85(3)$ GPa, $K'_a = 5(1)$, and $a_0 = 9.8660(9)$ Å; $K_{0b} = 113(2)$, $K'_b = 4.4(6)$, and $b_0 = 18.0548(6)$ Å; $K_{0c} = 107(3)$ GPa, $K'_c = 7(1)$, and $c_0 = 5.3185(5)$ Å for sample DL5. This suggests that the compressibility of kaersutite decreases with increasing oxo-component.

Structural refinements show that the polyhedral compressibility follows the order $A = M4 > M2 > M3 > M1$ for DL5 and $A = M4 > M2 > M1 > M3$ for FR12. The most evident geometrical effect induced by P is the decrease in the bending of the double tetrahedral chain, when adjacent I-beams are pushed against each other. This effect is largest for DL5, which has a larger concavity of the A site, (O7-O7' changes from 3.03 to 2.82 Å) compared to the one of FR12, (O7-O7' changes from 2.92 to 2.79 Å). This mechanism is confirmed by the evolution of T1-O7-T1 angle (from 135.4° to 132.5° in FR12 and from 136.6° to 132.2° in DL5).

Keywords: Oxo-amphiboles, kaersutite, compressibility, equation of state, high-pressure structure, amphibole

INTRODUCTION

Amphibole represents the most widespread hydrous mineral in the lithospheric mantle, where it plays a key role in controlling the petrologic and geochemical development of metasomatic processes (Vannucci et al. 1995; Ionov and Hofmann 1995; Ionov et al. 2002; Wallace and Green 1991; Niida and Green 1999). Furthermore, its breakdown is believed to be crucial for the genesis of alkaline melts (Halliday et al. 1995).

Amphiboles have a large stability field at high T - P conditions in both alkaline and calc-alkaline magmatic rocks (Irving and Green 2008; Alonso-Perez et al. 2009), making them widespread in rocks in both extensive and compressive settings, thus also strongly influencing the differentiation trends.

The role of amphibole breakdown to volatile recycling and arc magmatism is debated. In recent years, several experimental studies have constrained the P - T conditions of amphibole stability in subducting slabs with different chemical composition. Poli and Schmidt (1995) and Fumagalli and Poli (2005) argued that amphiboles are breaking down at about 2.5 GPa, thus releasing fluids in forearc settings. Based on experimental petrology,

the pressure stability of amphibole was recently extended to 3 GPa, which corresponds to 90–100 km depth (Forneris and Holloway 2003). This may directly link amphibole dehydration to the location of volcanic fronts which are typically located 90–150 vertical kilometers above the slab as marked by the Wadati-Benioff zone.

Amphiboles are also attracting special interest as critical indicators of physicochemical conditions for melt crystallization, such as pressure, water-pressure, temperature, and water activity. The assessment of these thermochemical and thermophysical properties is important for the calculation of phase equilibria.

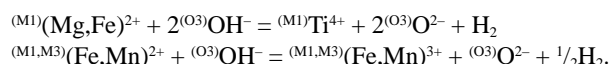
Extensive characterization of amphibole crystal chemistry has been carried out using diffraction and spectroscopic methods (Hawthorne et al. 2007 and references therein), relating changes in composition, cation ordering, and trace-elements behavior to petrogenetic conditions.

Oberti et al. (2007a, 2007b) showed that amphiboles with a significant oxo-component, i.e., with the (OH,F,Cl) content of the O3 site < 2 apfu, are quite common. The oxo-component is believed to be acquired by either primary crystallization or a post-crystallization oxidation process (dehydrogenation s.s.). The detection and quantification of the oxo-component is criti-

* E-mail: zanazzi@unipg.it

cal for the correct calculation of the unit formulae to be used for thermodynamic modeling or for the interpretation of trace element behavior (Tiepolo et al. 2007).

H-deficient calcic amphiboles in mantle and volcanic-arc environments have commonly titanian pargasite and kaersutite compositions. The degree of oxo-component is inversely correlated with the H₂O concentration of the parent melts (F and Cl content usually being very subordinate) and can be further increased by H loss (dehydrogenation processes). The consequent excess of negative charge at the O3 site is locally balanced by Ti at the M1 site and/or by the presence of Fe³⁺ at the same site or at the M3 site, according to two different crystal-chemical mechanisms (Tiepolo et al. 1999; Oberti et al. 2007a):



Detailed crystal-chemical settings were investigated extensively using a multi-technique approach: Mössbauer spectroscopy, EMP, SIMS, and single-crystal X-ray refinements (Zanetti et al. 1997, 2000). These studies indicated that, if Ti is strongly partitioned at the more distorted M1 site, Fe³⁺ may be partitioned over the two independent M1 and M3 sites. In particular, the distortion of M3 is not affected by the Ti occupancy, and therefore may give an indication of the presence of Fe³⁺ created by the dehydrogenation process.

In spite of the importance of amphiboles, relatively few studies on their structural behavior under non-ambient conditions have been made. Attention has been mainly focused on the thermal expansion and structural evolution with temperature, see for example the single-crystal diffraction studies on tremolite (Sueno et al. 1973), glaucophane (Jenkins and Corona 2006), richterite (Cameron et al. 1983; Cámara et al. 2003; Tribaudino et al. 2008), and kaersutite (Zema et al. 2009; Oberti et al. 2009b, 2009c). Recent research (Oberti et al. 2009b, 2009c) confirmed the speculation that the increase of the oxo-component enlarges the maximum *T* for pargasite-kaersutite stability (Tiepolo et al. 1999) due to the related decrease of the O-H bond, the weakest bond within the amphibole structure.

Nevertheless, the pressure effect on the structural evolution is not yet well constrained. To date, measurements of the compressibility and structure changes with pressure are scarce. Single-crystal in situ X-ray diffraction studies have been reported for tremolite, pargasite, and glaucophane up to 4 GPa (Comodi et al. 1991), and for grunerite up to 5.1 GPa (Zhang et al. 1992). The compressibility of synthetic K-richterite (Welch and Lennie, unpublished results reported in Welch et al. 2007) has been determined by the Rietveld method using synchrotron powder data. The compressibility of two polymorphs on the cummingtonite-grunerite join up to 8 GPa, and the effect of pressure on the *C2/m-P2₁/m* phase transition of cummingtonite have been reported (Yang et al. 1998; Boffa Ballaran et al. 2000).

Thus, to understand the effect of the oxo-component on the compressibility of amphibole, two natural kaersutite megacrysts (samples DL5 and FR12) from a basalt were studied by single-crystal X-ray diffraction using a diamond-anvil cell (DAC). These amphiboles are characterized by a very similar cation composition, apart from the Fe³⁺/(Fe²⁺+Fe³⁺) ratio, which according

to SREF+EMPA+SIMS data is 0.33 and 0.96 in DL5 and FR12, respectively (Table 1). Similar values of Fe³⁺/(Fe²⁺+Fe³⁺) ratio were obtained by means of Mössbauer investigation by Zanetti et al. (2000). The resulting oxo-component is different in the two samples (i.e., 1.1 apfu, DL5; 1.9 apfu, FR12).

In particular, the Ti content of our amphibole samples is very similar (0.53 to 0.59 apfu), so its contribution to the balance of the oxo-component is believed to be comparable in both samples. Owing to the prevalent ordering of Ti on M1 and Fe³⁺ on M2 found for DL5 (A. Zanetti, unpublished data), it is argued that in such a sample Ti plays the leading role in balancing the electrostatic requirements determined by the occurrence of O²⁻ at O3. According to the published partitioning coefficient ^{Amph}/_LD(H₂O) (Hauri et al. 2006), the H₂O content in DL5 reflects the chemical equilibrium with the parent melt. Conversely, the larger oxo-component and the associated oxidation of Fe in FR12 described by the Fe²⁺ + OH⁻ = Fe³⁺ + O²⁻ + 1/2H₂ substitution mechanism are attributed to a dehydrogenation process, which occurred during the transportation of the crystal toward the surface.

EXPERIMENTAL METHODS

Two natural kaersutites (FR12 and DL5), previously characterized by Zanetti et al. (2000) using a combined SREF, EMP, SIMS, and Mössbauer study, were selected for high-pressure X-ray diffraction experiments. FR12 originated from an alkaline basalt of the Massif Central, France, while DL5 has been extracted from an alkaline basalt of Deadman Lake Volcanic Area, U.S.A. (see also, Dyar et al. 1993). The chemical composition was determined with a Cameca SX100 microprobe, operating conditions were those described by Oberti et al. (2009a). The relative oxide percent by weight of the studied samples, as well as the chemical formulae, are reported in Table 1. According to the IMA amphibole nomenclature (Leake et al. 1997, 2003; Hawthorne and Oberti 2007a) amphibole DL5 is an oxygenian kaersutite, while the FR12 sample is an oxygenian ferri-kaersutite. For the sake of simplicity they are named here as kaersutite.

High-pressure lattice measurements

Unit-cell lattice parameters were measured at different pressures up to about 8 GPa by means of high-pressure single-crystal X-ray diffraction at the Bayerisches

TABLE 1. Representative analyses (wt%) and structural formulae of amphibole samples FR12 and DL5

	FR12	DL5		FR12	DL5
SiO ₂	39.56	39.62	Si	5.972	6.056
TiO ₂	5.15	4.64	Al	2.028	1.944
Al ₂ O ₃	13.80	13.54	Total T	8.000	2.000
Cr ₂ O ₃	0.03	0.01	Al	0.428	0.496
FeO _{tot}	10.45	11.82	Fe ³⁺	1.273	0.505
MnO	0.10	0.13	Ti	0.585	0.533
NiO	0.03	0.01	Cr	0.004	0.001
MgO	12.71	11.61	Ni	0.004	0.001
CaO	11.27	10.87	Mg	2.648	2.548
Na ₂ O	2.33	2.35	Fe ²⁺	0.047	0.914
K ₂ O	1.48	1.64	Mn ²⁺	0.013	-
H ₂ O	0.07	0.83	Total M1,2,3	5.000	5.000
F	0.09	0.04	Mg	0.210	0.095
Cl	0.03	0.04	Fe ²⁺	-	0.091
-O=F	0.04	0.03	Mn ²⁺	-	0.017
-O=Cl	0.01	0.01	Ca	1.790	1.780
Total	97.06	97.14	Na	-	0.016
			Total M4	2.000	2.000
			Ca	0.033	-
			Na	0.682	0.680
			K	0.285	0.320
			Total A	1.000	1.000
			OH	0.070	0.846
			F	0.043	0.034
			Cl	0.008	0.010
			O	1.879	1.110
			Total X	2.000	2.000

Geoinstitut, Bayreuth, using BGI design diamond-anvil cells (BGI-DAC, Allan et al. 1996), steel gaskets (T301) pre-indented to a thickness of about 100 μm and holes with diameters of 300 μm . The crystals were loaded together with a few ruby chips for pressure calibration (Mao et al. 1986) and a mixture of 4:1 methanol:ethanol as hydrostatic pressure medium. Unit-cell parameters were determined at each pressure by centering 12–17 Bragg reflections between 15° and 30° in 2 θ using a four-circle Huber diffractometer operating at 50 kV and 40 mA (MoK α). During the centering procedure, the effects of crystal offsets and diffractometer aberrations were eliminated from refined peak positions by the eight-position centering method of King and Finger (1979). The unit-cell parameter data of FR12 and DL5 samples at different pressures are reported in Table 2.

Room-pressure data collection

For the structure refinement at room conditions, crystal fragments of FR12 and of DL5 were mounted in air at Perugia University on an Xcalibur (Oxford Diffraction) diffractometer equipped with a CCD area detector operating at 50 kV and 35 mA using graphite monochromated Mo radiation (λ K α_1 = 0.7093 Å). To maximize the reciprocal space coverage, a combination of ω and ϕ scans was used, with a step size of 0.8° and an exposure time of 25 s/frame. Data were corrected for absorption with the program SADABS (Sheldrick 1996). Details of data collection for the investigated samples are listed in Table 3.

The crystal-structure refinements were carried out in the $C2/m$ space group with anisotropic displacement parameters using the SHELX-97 program (Sheldrick 1997), starting from the atomic coordinates of Tiepolo et al. (1999). Neutral atomic scattering factors and $\Delta f'$, $\Delta f''$ coefficients from *International Tables for Crystallography* (Wilson and Prince 1999) were used. Full occupancy was assumed for T1, T2, M1, M2, and M3 cation sites. The number of electrons in the cation sites was accounted for by fitting the scattering factor curves of Si at the tetrahedral sites and Mg against Fe for the octahedral sites, with variable occupancy (Table 4¹). Only partial occupancy was refined for M4 site (nominally occupied by Ca), the split M4' site (partially occupied by Fe) and A(m) and A2 (partially occupied by K and Na). The presence of H appeared on the difference Fourier map of the DL5 sample, and was inserted in the last stages of the refinement. The resulting sum of electrons for the cation sites were 246.98 and 251.06 e⁻ for FR12 and DL5, respectively, in good agreement with data calculated for the formula unit A₂M₄2M₁2M₂1M₃T₈O₂₂(O,OH)₂ on the basis of the chemical analysis (246.1 and 249.8 e⁻). No peak larger than 0.6 e⁻/Å³ was present in the final difference Fourier synthesis. Fractional atomic coordinates and displacement parameters (Å²) are listed in Table 4¹, whereas observed and calculated structure factors are reported in Table 5¹.

High-pressure data collections

For the structural study at high pressure, several samples of FR12 and DL5 amphiboles with dimensions of about 200 × 150 × 80 μm were chosen and used in several mountings. Each crystal was loaded in an ETH diamond anvil cell (DAC) (Miletich et al. 2000) equipped with type-I diamonds with 600 μm culet face diameter. The pressure chamber was a 300 μm diameter hole, drilled in a 250 μm thick steel Inconel 750 \times gasket pre-indented to 180 μm . A methanol:ethanol mixture (4:1) was used as hydrostatic pressure-transmitting medium. The experiments were carried out in the pressure range 10⁻⁴ to 6.4 GPa.

The DAC was mounted on a Xcalibur (Oxford Diffraction) diffractometer equipped with a CCD area detector, operating at 50 kV and 35 mA, and using graphite monochromated Mo radiation (λ K α_1 = 0.7093 Å). The DAC was centered on the diffractometer following the procedure of Budzianowski and Karusiak (2004). Intensity data were collected with the CCD detector. To maximize the reciprocal space coverage, a combination of ω and ϕ scans was used, with a step size of 0.8° and an exposure time of 50 s/frame. Lattice parameters were refined from the angles of the entire data set. The pressure calibration was based on the previously determined equation of state of the two amphiboles. Data were measured at 0.26, 2.85, 3.74, 4.31, 4.84, and 6.35 GPa for amphibole FR12, and at 0.67, 3.65, 4.54, and 5.42 GPa for DL5. The uncertainty on P was estimated to be less than ± 0.07 GPa. To improve the observation/parameter ratio, the determination of the structural parameters at 3.74 and 4.31 GPa for sample FR12 and at 3.65 and 5.42 GPa for sample DL5 has been carried out merging the reflections from two different mountings in the DAC at nearly the same pressure, after the relevant corrections.

The intensity data were corrected for the cell and crystal absorption using the Absorb V6.1 software (Angel 2004a). The least-squares refinements were performed with the SHELX-97 program (Sheldrick 1997). Isotropic atomic displacement parameters were used for all atoms and the site occupancies were

TABLE 2. Lattice parameters of FR12 and DL5 amphiboles as a function of P

P (GPa)	a (Å)	b (Å)	c (Å)	β (°)	$a \sin \beta$ (Å)	V (Å ³)
FR12						
10 ⁻⁴	9.816(3)	18.013(2)	5.301(2)	105.39(3)	9.464(3)	903.5(4)
0.44(5)	9.797(1)	17.9868(9)	5.2931(8)	105.46(1)	9.443(1)	899.0(2)
2.53(5)	9.728(2)	17.887(2)	5.262(1)	105.76(2)	9.362(2)	881.1(2)
2.98(5)	9.7143(6)	17.8655(8)	5.2579(4)	105.813(6)	9.347(1)	877.98(9)
3.56(5)	9.6959(7)	17.8385(9)	5.2496(4)	105.889(7)	9.325(1)	873.27(9)
4.06(5)	9.6833(8)	17.814(1)	5.2437(5)	105.937(9)	9.311(1)	869.8(1)
4.67(5)	9.6655(9)	17.7902(8)	5.2359(7)	106.009(9)	9.291(1)	865.4(1)
5.23(5)	9.6497(8)	17.764(1)	5.2290(4)	106.065(8)	9.273(1)	861.3(1)
6.08(5)	9.6274(7)	17.726(1)	5.2190(5)	106.153(8)	9.247(1)	855.5(1)
6.60(5)	9.6144(8)	17.7090(8)	5.2133(6)	106.198(9)	9.233(1)	852.4(1)
7.05(5)	9.6053(7)	17.6927(6)	5.2089(4)	106.231(7)	9.222(1)	849.93(9)
2.84(5)*	9.7175(9)	17.8742(6)	5.2596(4)	105.808(9)	9.350(1)	879.0(1)
DL5						
10 ⁻⁴	9.866(1)	18.0549(6)	5.3189(6)	105.20(1)	9.521(1)	914.3(2)
0.2(1)	9.857(1)	18.0424(8)	5.3137(8)	105.23(1)	9.511(1)	911.8(2)
0.69(5)	9.839(1)	18.0172(8)	5.3068(7)	105.34(1)	9.488(1)	907.3(2)
1.29(5)	9.819(5)	17.989(1)	5.298(1)	105.43(5)	9.465(5)	902.1(6)
2.40(5)	9.779(2)	17.9310(5)	5.2814(5)	105.60(2)	9.419(2)	892.0(3)
4.65(5)	9.705(5)	17.829(1)	5.252(1)	105.86(2)	9.336(5)	874.1(6)
5.90(5)	9.673(3)	17.7738(8)	5.2365(7)	105.98(4)	9.299(3)	865.4(3)
6.83(5)	9.644(6)	17.732(1)	5.225(1)	106.08(7)	9.267(6)	858.6(7)
7.70(5)	9.623(5)	17.700(1)	5.2161(9)	106.12(5)	9.245(5)	853.5(6)
8.12(5)	9.609(5)	17.682(1)	5.211(1)	106.17(5)	9.229(5)	850.3(6)
4.11(5)*	9.725(3)	17.8539(8)	5.2595(8)	105.81(4)	9.357(3)	878.7(4)

* Data points collected during decompression.

fixed to the values resulting from the refinement in air. Soft restraints on T-O bond distances and O-T-O angles were introduced in cases where the number of independent reflections was too low to increase the observation to parameter ratio. This is justified due to the observation that in silicates, the Si/Al tetrahedra do not undergo relevant changes in the investigated pressure range (Smyth et al. 2000). This was accomplished by imposing bond distances like those from the refinement in air, with a sigma of 0.02 Å, and refining the tetrahedra as quasi-rigid bodies. Details of data collections and refinement are listed in Table 3. Fractional atomic coordinates and displacement parameters are reported in Table 4¹. Observed and calculated structure factors are reported in Table 5¹.

RESULTS

Equation of state and compressibility

The evolution of the unit-cell parameters and of the unit-cell volumes as a function of pressure for the two samples is documented in Table 2 and shown in Figures 1 and 2. They show a steady change as a function of pressure. No evidence for phase transitions was found in the investigated pressure range. In particular, all the cell axes decrease monotonously, whereas the β angle increases with pressure.

The “normalized stress” F_E vs. the Eulerian finite strain f_E (Jeanloz and Hazen 1991; Angel 2000) indicates that K' is larger than 4 for both samples (Fig. 3). Therefore, third-order Birch-Murnaghan Equation of State (BM3-EoS) has been used to fit the pressure-volume (P - V) data of both samples refining simultaneously the unit-cell volume at room pressure, V_0 , the bulk modulus, K_{T0} , and its first pressure derivative, K' , using the EOS-FIT V6.1 program (Angel 2004b). The resulting EoS parameters are the following: $K_{T0} = 94(2)$ GPa, $K' = 6.5(8)$, and

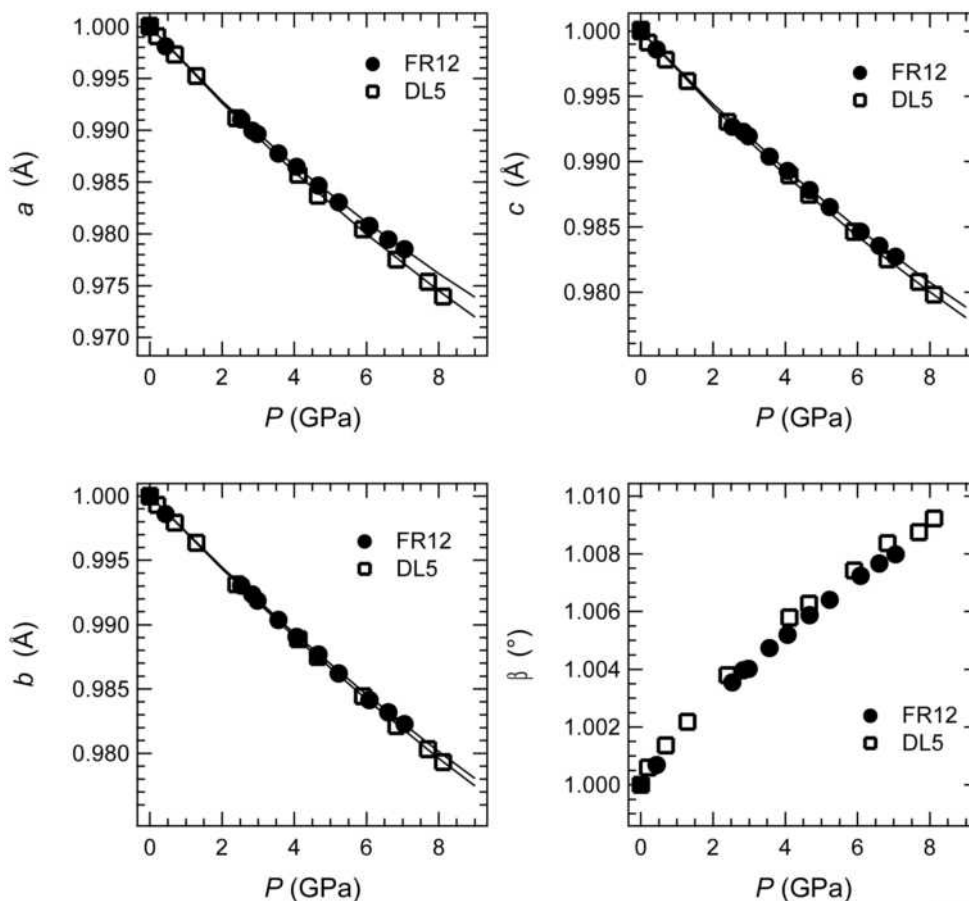
¹ Deposit item AM-10-028, Tables 4 and 5. Deposit items are available two ways: For a paper copy contact the Business Office of the Mineralogical Society of America (see inside front cover of recent issue) for price information. For an electronic copy visit the MSA web site at <http://www.minsocam.org>, go to the *American Mineralogist* Contents, find the table of contents for the specific volume/issue wanted, and then click on the deposit link there.

TABLE 3. Details of data collection and refinement of FR12 and DL5 samples at various pressures

P (GPa)	0.0001*	0.26	2.85	3.74	4.31	4.84	6.35
			FR12				
<i>a</i> (Å)	9.816(1)	9.807(2)	9.718(2)	9.691(2)	9.675(2)	9.660(3)	9.620(3)
<i>b</i> (Å)	18.013(1)	17.999(3)	17.870(3)	17.831(3)	17.804(3)	17.781(5)	17.717(5)
<i>c</i> (Å)	5.300(1)	5.296(2)	5.259(2)	5.247(2)	5.240(2)	5.233(2)	5.216(2)
β (°)	105.38(1)	105.4(1)	105.8(1)	105.9(1)	106.0(1)	106.0(2)	106.2(2)
<i>V</i> (Å ³)	903.65(6)	901.1(1)	878.8(2)	871.9(1)	867.7(1)	863.9(2)	853.8(2)
θ range	3–40°	3–30°	3–30°	3–30°	3–30°	3–30°	3–30°
Crystal-detector distance (mm)	65	65	65	65	65	65	65
No. measured reflections	13242	3698	2487	6778	3464	1746	1734
No. indep. reflections	2840	555	426	530	343	260	264
Reflections with $I > 4\sigma(I)$	1872	428	293	381	219	172	128
No. refined parameters	116	49	53	50	51	33†	33†
R_{int} %	4.6	5.5	10.3	9.6	9.4	7.6	11.9
R_1 %	2.7	3.8	7.1	5.6	6.3	6.3	9.9
P (GPa)	0.0001*	0.67	3.65	4.54	5.42		
			DL5				
<i>a</i> (Å)	9.866(1)	9.841(2)	9.737(2)	9.710(2)	9.685(2)		
<i>b</i> (Å)	18.054(1)	18.019(3)	17.873(3)	17.833(3)	17.794(3)		
<i>c</i> (Å)	5.318(1)	5.307(2)	5.264(2)	5.253(2)	5.242(2)		
β (°)	105.22(1)	105.3(1)	105.8(1)	105.9(1)	105.9(1)		
<i>V</i> (Å ³)	914.02(6)	907.6(1)	881.7(2)	875.0(2)	868.6(2)		
θ range	3–30°	3–30°	3–30°	3–30°	3–30°		
Crystal-detector distance (mm)	65	65	65	65	65		
No. measured reflections	3772	1195	3497	1664	3344		
No. indep. reflections	1448	190	322	259	329		
Reflections with $I > 4\sigma(I)$	1265	142	198	167	187		
N° refined parameters	117	36†	37†	36†	37†		
R_{int} %	1.6	6.5	8.0	7.6	10.0		
R_1 %	1.9	4.6	6.4	7.6	6.4		

* Data collected with the sample in air.

† This refinement was performed imposing some constraints on atomic thermal displacements and the geometry of Si tetrahedra (see text).

**FIGURE 1.** Unit-cell parameters of FR12 and DL5 samples as a function of pressure. The data are normalized with respect to the room-pressure values. Estimated standard deviations are smaller than symbols. Solid lines are linearized third-order Birch Murnaghan EoS fits through the data.

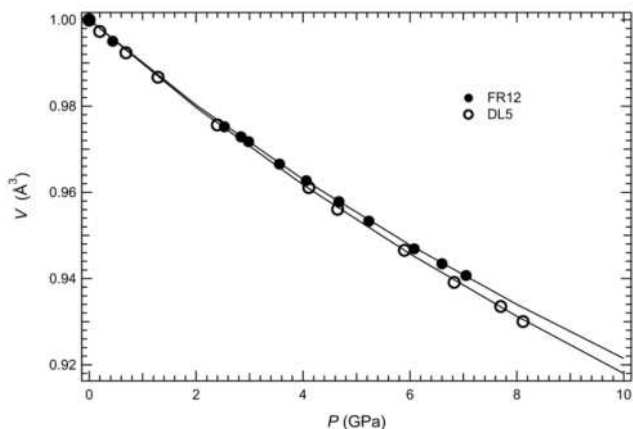


FIGURE 2. Variation with pressure of the unit-cell volumes of FR12 and DL5 samples. The data are normalized with respect to the room-pressure values. Estimated standard deviations are smaller than symbols. Solid lines are third-order Birch Murnaghan EoS fits through the data.

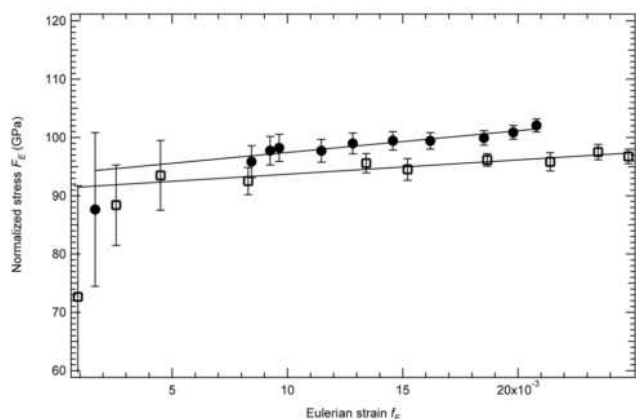


FIGURE 3. Plot of normalized stress, defined as $F_E = P/[3f_E(1 + 2f_E)^{5/2}]$ vs. finite strain $f_E = [(V_0/V)^{2/3} - 1]/2$ for FR12 (full circles) and DL5 (open squares) samples. Solid lines are weighted linear fits through the data resulting in the following expressions: $F_E = 94(2) + 374(124)f_E$ and $F_E = 91(2) + 245(109)f_E$ for FR12 and DL5, respectively.

$V_0 = 903.4(3) \text{ \AA}^3$ for FR12 sample and $K_{70} = 92(2) \text{ GPa}$, $K' = 5.6(9)$, and $V_0 = 914.1(2) \text{ \AA}^3$ for DL5 sample. These values are in good agreement with those that can be obtained from weighted linear fits through the F - f data.

The axial moduli of the two amphibole samples were also calculated using a parameterized form of the BM3-EoS in which the individual axes are cubed and fitted as volumes using the program EOS-FIT V6.1 (Angel 2004b). The resulting EoS parameters are the following: $K_{0a} = 86(3) \text{ GPa}$, $K'_a = 7(1)$, and $a_0 = 9.815(2) \text{ \AA}$; $K_{0asin\beta} = 71(1) \text{ GPa}$, $K'_{asin\beta} = 6.5(4)$, and $asin\beta_0 = 9.463(2) \text{ \AA}$; $K_{0b} = 115(3) \text{ GPa}$, $K'_b = 4.8(8)$, and $b_0 = 18.012(2) \text{ \AA}$; $K_{0c} = 112(5) \text{ GPa}$, $K'_c = 7(1)$, and $c_0 = 5.300(1) \text{ \AA}$ for sample FR12 and $K_{0a} = 85(3) \text{ GPa}$, $K'_a = 5(1)$, and $a_0 = 9.8660(9) \text{ \AA}$; $K_{0asin\beta} = 69(1) \text{ GPa}$, $K'_{asin\beta} = 5.1(5)$, and $asin\beta_0 = 9.520(2) \text{ \AA}$; $K_{0b} = 113(2)$, $K'_b = 4.4(6)$, and $b_0 = 18.0548(6) \text{ \AA}$; $K_{0c} = 107(3) \text{ GPa}$, $K'_c = 7(1)$, and $c_0 = 5.3185(5) \text{ \AA}$ for sample DL5. The axial compressibility, obtained with the relation $\beta = -1/3K_0^{-1}$ and expressed in 10^{-3} GPa^{-1} , is as follows: $\beta_a = -3.88$, $\beta_{asin\beta} = -4.14$, $\beta_b = -2.90$, $\beta_c = -2.98$ for FR12; $\beta_a = -3.92$, $\beta_{asin\beta} = -4.10$, $\beta_b = -2.95$, $\beta_c = -3.12$ for DL5. This shows that the largest compressibility is along $[100]$.

The strain tensors for the two samples and their orientation in relation to the crystallographic axes were calculated with the program of Ohashi (1982). The principal components and their orientation over a pressure range of about 7 GPa are reported in Table 6. The intermediate strain component, ϵ_2 , is coincident with the **b** axis while the maximum, ϵ_1 , and minimum, ϵ_3 , strain components lie in the (010) plane; the direction ϵ_1 forms an angle of about 62° with the *c* lattice parameter and about 44° with the **a** axis (Fig. 4). The unit-strain tensor components of the two samples are very similar, in agreement with their similar chemical composition: the ratios between the ellipsoid axes are 1:0.60:0.45 and 1:0.61:0.52 for FR12 and DL5, respectively.

Structural evolution with pressure

Bond lengths, variations of polyhedral volumes and distortion coefficients of FR12 and DL5 samples as a function of pressure are listed in Tables 7 and 8 respectively. The compressibility coefficients ($\beta = \Delta V/V\Delta P$) of A, M1, M2, M3, and M4 polyhedra are listed in Table 9. The coefficients were calculated by linear least-squares fitting of polyhedral volumes against *P*.

The structural refinements show that the M4 and A polyhedra are the softest in both samples. The compressibility order of the M polyhedra is $M4 > M2 > M3 > M1$ in DL5 and $M4 > M2 > M1 > M3$ in FR12.

The M4 polyhedra are softer than the other M1, M2, and M3 polyhedra in both samples studied (Table 9). Crystal-chemical studies of amphiboles (Hawthorne and Oberti 2007b) have shown

TABLE 6. Principal components and direction of the unit-strain ellipsoids

Parameter	DL5	FR12
ϵ_1 (GPa^{-1})	$4.2(8) \cdot 10^{-3}$	$4.2(2) \cdot 10^{-3}$
ϵ_2 (GPa^{-1})	$2.56(8) \cdot 10^{-3}$	$2.54(6) \cdot 10^{-3}$
ϵ_3 (GPa^{-1})	$2.2(5) \cdot 10^{-3}$	$1.9(1) \cdot 10^{-3}$
Θ ($^\circ$)*	62.2(2)	61.1(3)

* Angle Θ between ϵ_1 and the *c* axis (positive value between the *c* axis and the positive *a* axis).

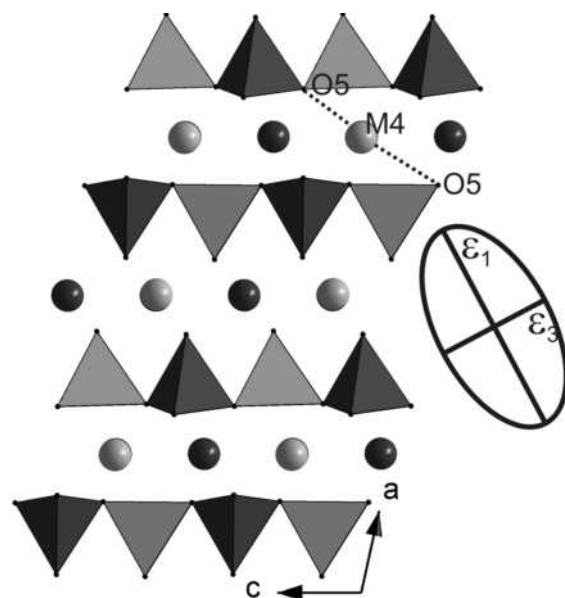


FIGURE 4. The structure of kaersutite projected along $[010]$ and the strain ellipses.

TABLE 7. Relevant bond lengths (Å), polyhedral volumes, and distortion coefficients (following Robinson et al. 1971) of FR12 sample at various pressures

P (GPa)	0.0001	0.26	2.85	3.74	4.31	4.84	6.35
T1-O1	1.676(1)	1.669(6)	1.64(1)	1.64(1)	1.66(2)	1.67(2)	1.68(2)
T1-O5	1.681(1)	1.681(4)	1.69(1)	1.673(7)	1.67(1)	1.70(1)	1.71(2)
T1-O6	1.677(1)	1.682(4)	1.66(1)	1.672(7)	1.65(1)	1.68(1)	1.69(2)
T1-O7	1.661(1)	1.663(3)	1.65(1)	1.657(6)	1.66(1)	1.65(1)	1.63(1)
<T1-O>	1.674	1.67	1.66	1.66	1.66	1.67	1.67
V (Å ³)	2.402(4)	2.40(5)	2.36(4)	2.35(3)	2.34(4)	2.40(4)	2.41(9)
λ*	1.001	1.002	1.002	1.001	1.001	1.001	1.002
σ ² †	5.25	6.36	6.28	5.92	4.57	4.82	6.18
T2-O2	1.642(1)	1.634(6)	1.60(2)	1.62(1)	1.62(2)	1.64(2)	1.62(2)
T2-O4	1.609(1)	1.610(5)	1.59(1)	1.597(7)	1.60(1)	1.60(1)	1.62(2)
T2-O5	1.643(1)	1.651(4)	1.63(1)	1.638(7)	1.64(1)	1.62(1)	1.60(2)
T2-O6	1.656(1)	1.652(4)	1.66(1)	1.641(6)	1.65(1)	1.66(1)	1.65(1)
<T2-O>	1.637	1.64	1.62	1.62	1.63	1.63	1.62
V (Å ³)	2.239(4)	2.24(5)	2.18(4)	2.19(3)	2.20(4)	2.21(4)	2.18(9)
λ*	1.004	1.004	1.003	1.004	1.003	1.003	1.005
σ ² †	17.22	18.15	13.69	15.06	13.10	13.19	21.08
M1-O1(x2)	2.044(1)	2.043(4)	2.05(1)	2.033(7)	2.026(9)	2.03(1)	2.01(1)
M1-O2(x2)	2.173(1)	2.166(5)	2.15(1)	2.129(7)	2.13(1)	2.12(1)	2.14(2)
M1-O3(x2)	1.946(1)	1.958(5)	1.92(1)	1.945(8)	1.93(1)	1.94(2)	1.90(3)
<M1-O>	2.054	2.056	2.043	2.039	2.029	2.028	2.016
V (Å ³)	11.29(1)	11.33(8)	11.2(1)	11.1(1)	10.9(1)	10.9(1)	10.6(3)
λ*	1.018	1.017	1.016	1.013	1.016	1.016	1.020
σ ² †	53.10	49.07	44.73	38.20	47.40	47.51	59.05
M2-O1(x2)	2.117(1)	2.118(5)	2.12(1)	2.107(7)	2.09(1)	2.07(1)	2.04(2)
M2-O2(x2)	2.085(1)	2.084(4)	2.08(1)	2.072(7)	2.06(1)	2.04(1)	2.05(2)
M2-O4(x2)	1.973(1)	1.973(5)	1.99(1)	1.968(8)	1.96(1)	1.94(1)	1.89(2)
<M2-O>	2.058	2.058	2.062	2.049	2.033	2.023	2.00
V (Å ³)	11.46(1)	11.46(8)	11.5(1)	11.3(1)	11.8(1)	10.9(1)	10.5(3)
λ*	1.011	1.010	1.010	1.010	1.007	1.011	1.010
σ ² †	32.84	32.06	30.71	30.96	24.42	33.65	28.45
M3-O1(x4)	2.061(1)	2.060(5)	2.04(2)	2.036(7)	2.04(1)	2.04(1)	2.03(2)
M3-O3(x2)	2.035(1)	2.036(6)	2.02(2)	2.049(9)	2.02(1)	2.05(2)	2.03(3)
<M3-O>	2.052	2.052	2.033	2.041	2.033	2.034	2.032
V (Å ³)	11.16(1)	11.18(8)	10.9(1)	11.1(1)	10.9(1)	10.9(1)	10.8(3)
λ*	1.022	1.020	1.017	1.015	1.019	1.018	1.024
σ ² †	68.26	64.05	54.46	49.15	61.43	57.70	75.94
M4-O2(x2)	2.416(1)	2.420(5)	2.42(1)	2.397(7)	2.40(1)	2.39(1)	2.37(2)
M4-O4(x2)	2.342(1)	2.338(5)	2.34(1)	2.395(7)	2.33(1)	2.33(1)	2.30(2)
M4-O5(x2)	2.637(2)	2.624(5)	2.42(1)	2.552(7)	2.52(1)	2.49(1)	2.47(2)
M4-O6(x2)	2.537(1)	2.535(5)	2.53(1)	2.535(7)	2.53(1)	2.52(1)	2.52(2)
<M4-O>	2.485	2.48	2.45	2.45	2.44	2.43	2.40
V (Å ³)	14.09(1)	13.97(8)	13.5(1)	13.4(1)	13.3(1)	13.1(1)	12.7(3)
λ*	1.286	1.287	1.285	1.286	1.287	1.285	1.290
σ ² †	746.30	747.60	731.46	739.01	736.69	730.01	738.33
A-O5(x4)	3.048(1)	3.046(5)	3.09(1)	3.048(7)	3.07(1)	3.08(1)	3.10(2)
A-O6(x4)	3.071(1)	3.061(5)	3.00(1)	2.981(7)	2.98(1)	2.93(1)	2.91(2)
A-O7(x2)	2.404(1)	2.395(5)	2.32(1)	2.340(7)	2.33(1)	2.30(1)	2.31(2)
<A-O>	2.928	2.92	2.90	2.88	2.88	2.86	2.87
V (Å ³)	44.91(5)	44.6(2)	42.9(4)	42.1(3)	42.3(4)	41.1(4)	41.0(9)
M1-M1	2.869(1)	2.882(4)	2.85(1)	2.850(5)	2.845(9)	2.84(1)	2.79(2)
M1-M2	3.178(1)	3.170(2)	3.145(4)	3.134(2)	3.129(4)	3.127(5)	3.122(8)
O4-O4'§	2.568(2)	2.57(1)	2.62(1)	2.57(1)	2.58(1)	2.56(1)	2.41(1)
O7-O7'§	2.925(2)	2.91(1)	2.76(1)	2.79(1)	2.79(1)	2.78(1)	2.78(1)
α (°)‡	17.81(6)	18.2(1)	21.1(1)	20.4(1)	21.6(1)	23.3(2)	23.7(2)

* λ is the quadratic elongation.

† σ² is the angle variance (deg²).

‡ α is the tetrahedral rotation angle; see text for definition.

§ These distances are the components of O4-O4' and O7-O7' along the [100] direction.

TABLE 8. Relevant interatomic distances (Å), polyhedral volumes, and distortion coefficients (following Robinson et al. 1971) of DL5 sample at various pressures

P (GPa)	0.0001	0.67	3.65	4.54	5.42
T1-O1	1.670(1)	1.67(1)	1.68(1)	1.69(1)	1.67(1)
T1-O5	1.684(1)	1.68(1)	1.67(1)	1.69(1)	1.69(1)
T1-O6	1.680(1)	1.69(1)	1.68(1)	1.68(1)	1.67(1)
T1-O7	1.664(1)	1.66(1)	1.65(1)	1.65(1)	1.66(1)
<T1-O>	1.674	1.67	1.67	1.68	1.67
V (Å ³)	2.404(4)	2.40(4)	2.40(4)	2.42(4)	2.39(4)
λ*	1.001	1.001	1.001	1.001	1.001
σ ² †	5.03	5.65	3.42	3.34	5.44
T2-O2	1.641(1)	1.63(1)	1.62(1)	1.62(1)	1.62(1)
T2-O4	1.610(1)	1.60(1)	1.61(1)	1.60(1)	1.62(1)
T2-O5	1.648(1)	1.65(1)	1.61(1)	1.62(2)	1.62(1)
T2-O6	1.662(1)	1.65(1)	1.66(1)	1.68(1)	1.65(1)
<T2-O>	1.640	1.63	1.63	1.63	1.63
V (Å ³)	2.251(4)	2.21(4)	2.19(4)	2.19(4)	2.20(4)
λ*	1.004	1.004	1.005	1.005	1.005
σ ² †	17.23	16.86	19.45	21.68	19.34
M1-O1(x2)	2.048(1)	2.04(1)	2.02(1)	2.02(2)	2.02(1)
M1-O2(x2)	2.152(1)	2.15(1)	2.12(1)	2.11(2)	2.11(1)
M1-O3(x2)	2.027(1)	2.06(1)	2.04(2)	2.06(2)	2.03(2)
<M1-O>	2.076	2.08	2.06	2.06	2.06
V (Å ³)	11.68(2)	11.9(2)	11.4(2)	11.6(3)	11.4(2)
λ*	1.015	1.011	1.013	1.010	1.012
σ ² †	45.85	35.09	40.40	32.19	37.85
M2-O1(x2)	2.102(1)	2.11(1)	2.08(1)	2.08(2)	2.06(1)
M2-O2(x2)	2.078(1)	2.07(1)	2.05(1)	2.04(2)	2.04(1)
M2-O4(x2)	1.975(1)	1.97(1)	1.94(1)	1.94(2)	1.92(1)
<M2-O>	2.052	2.05	2.02	2.02	2.01
V (Å ³)	11.37(2)	11.3(2)	10.9(2)	10.8(3)	10.6(2)
λ*	1.009	1.010	1.010	1.011	1.010
σ ² †	28.40	30.50	30.30	33.28	29.51
M3-O1(x4)	2.084(1)	2.05(1)	2.04(1)	2.03(2)	2.02(1)
M3-O3(x2)	2.082(1)	2.13(2)	2.08(2)	2.13(3)	2.10(2)
<M3-O>	2.083	2.08	2.05	2.06	2.05
V (Å ³)	11.65(2)	11.7(2)	11.2(2)	11.4(3)	11.2(2)
λ*	1.023	1.020	1.020	1.018	1.019
σ ² †	72.71	61.12	63.47	56.31	60.28
M4-O2(x2)	2.412(2)	2.40(1)	2.38(1)	2.39(2)	2.35(1)
M4-O4(x2)	2.335(1)	2.34(1)	2.31(2)	2.29(2)	2.27(1)
M4-O5(x2)	2.656(1)	2.64(1)	2.59(1)	2.54(2)	2.53(1)
M4-O6(x2)	2.564(2)	2.57(1)	2.56(1)	2.59(2)	2.60(1)
<M4-O>	2.493	2.49	2.46	2.44	2.43
V (Å ³)	14.16(2)	14.1(2)	13.5(2)	13.2(3)	12.9(2)
λ*	1.290	1.293	1.292	1.297	1.300
σ ² †	758.37	764.05	758.14	757.50	804.51
A-O5(x4)	3.050(1)	3.06(1)	3.07(1)	3.07(2)	3.08(2)
A-O6(x4)	3.085(1)	3.07(1)	2.99(1)	2.94(2)	2.96(2)
A-O7(x2)	2.444(1)	2.45(1)	2.38(1)	2.34(2)	2.32(2)
<A-O>	2.943	2.94	2.90	2.87	2.88
V (Å ³)	46.09(5)	46.0(5)	43.3(5)	42.2(9)	42.4(5)
M1-M1	3.061(1)	3.06(1)	3.02(1)	2.98(2)	2.99(1)
M1-M2	3.143(1)	3.132(4)	3.108(4)	3.115(6)	3.095(4)
O4-O4'§	2.545(2)	2.54(1)	2.49(1)	2.48(2)	2.43(1)
O7-O7'§	3.032(2)	3.10(1)	2.93(1)	2.88(2)	2.82(1)
α (°)‡	17.74(7)	18.7(2)	19.9(2)	17.8(3)	23.1(3)

* λ is the quadratic elongation.

† σ² is the angle variance (deg²).

‡ α is the tetrahedral rotation angle; see text for definition.

§ These distances are the components of O4-O4' and O7-O7' along the [100] direction.

that the M4 site is significantly affected by the requirements of dimensional matching between the octahedral strip and the tetrahedral double-chain. In fact, while there is no correlation between the <M4-O> bond length and the mean radius of the cations occupying the M4 site (<r^{M4}>), there is a significant posi-

tive correlation of <M4-O> with the mean radius of cations in M1, M2, and M3 sites [<r^{M(1,2,3)}>]. In both samples of kaersutites, the <M4-O> bond distance decreases with pressure at about the same rate following the reduction of <r^{M(1,2,3)}>. Moreover, it is observed that the largest reduction is found for the longest

TABLE 9. Compressibility coefficients ($\text{GPa}^{-1} \times 10^3$) of polyhedra in FR12 and DL5 samples

β polyhedron	FR12	DL5
M1	-10(1)	-5(2)
M2	-12(3)	-12(1)
M3	-5(1)	-7(2)
M4	-15(1)	-16(1)
A	-14(1)	-17(2)

M4-O5 bonds (Tables 7 and 8). In $C2/m$ amphibole, the M4 site is surrounded by eight oxygen atoms, not all of which belong to its first coordination sphere. As the pressure increases, the M4-O5 distance of kaersutite decreases significantly and the coordination of M4 site becomes effectively eightfold. The strong reduction of M4-O5 distances controls the orientation of the strain ellipsoid, in fact this bond forms an angle of about 60° with the c axis (Fig. 4).

The M2 polyhedron has approximately the same compressibility for both samples (Table 9), whereas major difference is found for the relative compressibility of the M1 and M3 polyhedra. A large difference in compressibility is observed for the M3 octahedron, likely due to the different content in Fe^{3+} , with the M3 octahedron of FR12 being the stiffest between the two samples (Table 9). The M1 octahedron is more compressible in FR12 than in DL5, although its volume is larger for DL5 than for FR12 (Tables 7 and 8). This behavior may be explained by the significantly larger distortion of M1 in FR12, which has a higher Fe^{3+} occupation than DL5, and/or the need of maintaining the match with the edge shared with M4.

The two major movements in the tetrahedral ribbon concern the bending along the [100] direction through the A site and the tetrahedral rotation, necessary to maintain the coherence with the octahedral layer, whose size decreases with increasing P . Each individual double chain loses the slight concavity around the A site, becoming flatter. The reduction of the concavity of the double tetrahedral chain can be measured by the shortening of the projection of O7-O7' distance in the [100] direction, compared with the decrease of the component of O4-O4' distance along a (Tables 7 and 8; Fig. 5). In FR12, the O7-O7' distance decreases by 5.1%, from 2.925(2) Å at 1 atm to 2.78(1) Å at

6.4 GPa, while the O4-O4' distance decreases by 6.3%, from 2.568(2) to 2.41(1) Å. The difference $\Delta = [\text{O7-O7}'] - [\text{O4-O4}'] = 0.36$ Å remains practically constant as the pressure increases. In DL5, the same distances change from 3.032(2) and 2.545(2) Å to 2.82(1) and 2.43(1) Å at 5.4 GPa (6.9 and 4.4%, respectively) and the difference Δ decreases from 0.49 to 0.39 Å, with a consequent decrease in the bending of the tetrahedral chains. The same mechanism is outlined by the evolution of T1-O7-T1 angle [from $135.4(1)^\circ$ to $132.5(4)^\circ$ in FR12 and from $136.6(1)^\circ$ to $132.2(4)^\circ$ in DL5]. The increase of pressure also affects the tetrahedral rotation α , defined as the half of the difference between the average of the three larger and the three smaller O-O-O angles in the pseudo-hexagon of the double tetrahedral chain. In both samples α increases, from $17.81(6)^\circ$ to $23.7(2)^\circ$ and from $17.74(7)^\circ$ to $23.1(3)^\circ$ at 5.42 GPa for DL5 (Tables 7 and 8). The tetrahedral rotation explains the strong reduction of the M4-O5 distance, from 2.637(2) to 2.47(2) Å at 6.35 GPa for FR12 and from 2.656(1) to 2.53(1) Å at 5.42 GPa for DL5.

DISCUSSION

Effect of the oxo-component on the compressibility of kaersutites

The bulk moduli and pressure derivative of the two kaersutite samples studied in this work show only small differences. However, both the F - f plot (Fig. 3) and the confidence ellipses constructed for the two samples (Fig. 6) to take into account the large correlation between the K_{0T} and the K' values suggest that this difference is real, and therefore the oxo-component appears to slightly stiffen the amphibole structure. Moreover, given that K' appears larger for FR12 than for DL5, we can expect that the difference in compressibility between the two samples will increase with pressure. This difference in compressibility is likely due to the compression behavior of the a axis. Although the “linearized” bulk modulus of this direction is practically the same for both samples, its first pressure derivative, K' , is much larger for sample FR12, implying that in this sample the a axis becomes much stiffer with increasing pressure than the a axis of the DL5 sample. The compressibility of the b and c axes, as well as the components of the strain tensor show similar behavior

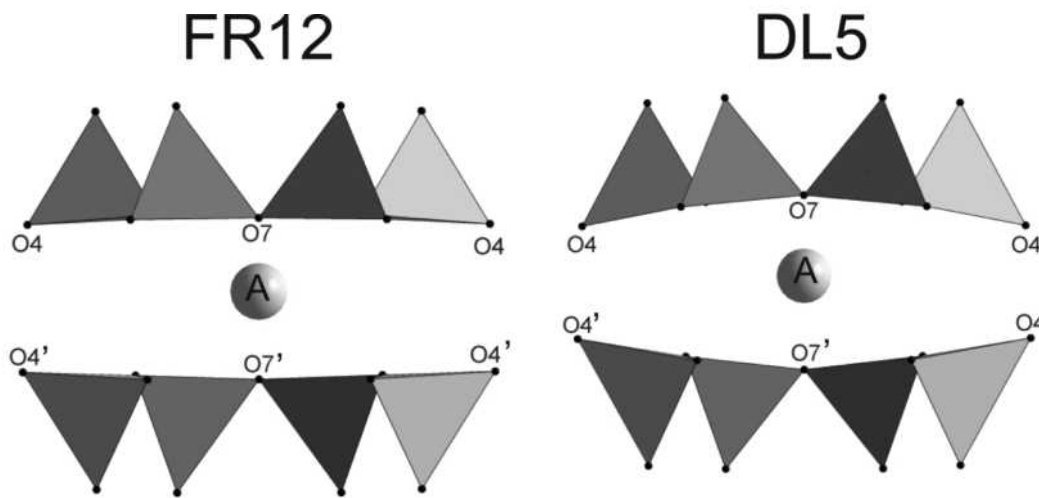


FIGURE 5. The double chains of FR12 and DL5 samples viewed along [001]. (The vertical tetrahedral displacement is exaggerated for sake of clarity).

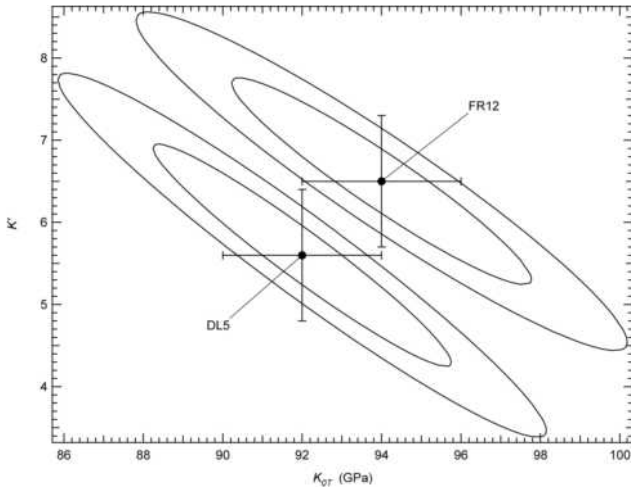


FIGURE 6. Confidence ellipses in K_0 and K' parameter space for the BM3-EoS fits. The error bars correspond to 1 e.s.d. of each of the individual parameters while the inner and outer ellipses show the regions of 68.3 and 95.4% confidence level for both parameters, respectively.

for both samples. The bending of the tetrahedral double-chains appears to determine the different compressibility between the two samples of this study. The larger bending of DL5 sample is likely due to the electrostatic repulsion between the H linked to the O3 atoms and the A site, while the bending is reduced in FR12 even at ambient condition because of the attractive interaction between $\text{O}3^{2-}$ and the A site. At high pressure, the bending decreases more when the site O3 is occupied by the hydroxyl group, and as a consequence the DL5 sample is slightly more compressible than the FR12 sample.

To better compare our results with those reported in the literature for other amphiboles for which mostly the K' has been fixed to 4, the bulk moduli of FR12 and DL5 were recalculated using a second-order Birch-Murnaghan Equation of State. The following EoS parameters were obtained: $V_0 = 902.8(3) \text{ \AA}^3$, $K_{70} = 100.5(8) \text{ GPa}$ for sample FR12 and $V_0 = 914.1(2) \text{ \AA}^3$, $K_{70} = 96.8(7) \text{ GPa}$ for sample DL5 (Table 10). Kaersutite is much less compressible than tremolite, cummingtonite, and grunerite, and slightly less compressible than glaucophane, pargasite, and K-richterite (Table 10). In particular [see Table 2 in Welch et al. (2007)], the larger variation appears to occur for the a axis, while the variation of the other lattice parameters is more limited (with the exception for the $P2_1/n$ amphiboles). This is clearly an effect of chemical composition: amphiboles with the A site empty (tremolite, cummingtonite, and grunerite) are much more compressible than those with a filled A site (pargasite, K-richterite, and kaersutite).

A closer comparison between the elastic properties of kaersutites can be made with pargasite investigated by Comodi et al. (1991), which had virtually no oxo-component and the A site almost completely occupied by Na. The HP behavior of these amphiboles is controlled by the compressibility of the A site and the different response of the bending deformation of the double tetrahedral chain. At ambient P , the differences between the component along $[100]$ of the O7-O7' and O4-O4' distances (Fig. 5) are 0.54 Å for pargasite, 0.49 Å for DL5, and 0.36 Å for FR12, respectively. The variation of the component along $[100]$ of O4-

O4' distance with P is $0.02 \text{ \AA GPa}^{-1}$ for all the three samples, but that of O7-O7' is $0.07 \text{ \AA GPa}^{-1}$ for pargasite, $0.04 \text{ \AA GPa}^{-1}$ for DL5 and $0.02 \text{ \AA GPa}^{-1}$ for FR12. Therefore the deformation can be explained by the combined effect of two factors: (1) the shape of the cavity related to the bending of the two tetrahedral chains, which is a function of the oxo-component; and (2) the compressibility of the cation in the A position, which is greater for Na in pargasite than for K in kaersutite.

The compression effects arising from the volume reduction of M1, M2, M3 polyhedra for both samples studied are small and mainly due to compositional variation. The sequences of compressibility for the M octahedra in other amphiboles reported in the literature are $M3 > M1 > M2$ in glaucophane and $M2 > M1 > M3$ in tremolite and pargasite (Comodi et al. 1991), showing that the compressibility of the various components of the cation polyhedral layer strictly depends on the composition.

The maximum strain component is along a direction intermediate between that of M4-O5 bond, which has the largest compressibility in both samples, and the direction of \mathbf{a}^* (Fig. 4). The strain tensor of pargasite was calculated from the data of Comodi et al. (1991). The values of the principal components are 4.9×10^{-3} , 2.7×10^{-3} , and $2.2 \times 10^{-3} \text{ GPa}^{-1}$ similar to the values of kaersutites (Table 6). The largest axis forms an angle of 77° with the c axis. This orientation is different from that found in tremolite and glaucophane, for which the angle with the c axis is about 82° [see Table 4 in Tribaudino et al. (2008)]. Therefore the strain ellipses rotate toward \mathbf{a}^* forming angles of 8° in tremolite and glaucophane, 13° in pargasite, and 29° in kaersutite, owing to the different compressibility of the A site.

Comparison with the data of Zema et al. (2009) and Oberti et al. (2009b) on the thermal behavior of FR12 and DL5 kaersutites shows that the effects of P and T on the behavior of these amphiboles are only approximately inverse revealing therefore that the mechanism involved in the HP and in the HT deformations is different. For both samples, the expansion coefficients are $\alpha_b > \alpha_c > \alpha_a$, i.e., the major deformation is along the \mathbf{b} axis, while the major compression is along the \mathbf{a} axis. However, the thermal behavior of DL5 in the range 500–650 °C, before the dehydration process, shows that the hydroxyl group affects the expandability of the c axis and the β angle.

Based on our data, an inverse relationship between the water content and the bulk moduli of amphiboles can be postulated. In fact, the comparison of the bulk moduli of FR12 and DL5 kaersutites with pargasite studied by Comodi et al. (1991) shows that

TABLE 10. Bulk moduli (K_{70}) and their pressure-derivative K' of some amphiboles

Amphibole	K_{70} GPa	K'	Reference
Tremolite	76(3)	4	Comodi et al. (1991)
Pargasite	89(3)	4	Comodi et al. (1991)
Glaucophane	88(6)	4	Comodi et al. (1991)
K-richterite	89(3)	4	Welch et al. (2007)
Cummingtonite $P2_1/m$	62.4(5)	8.2(2)	Boffa Ballaran et al. (2000)
Cummingtonite $C2/m$	66(2)	8.2	Boffa Ballaran et al. (2000)
Cummingtonite $P2_1/m$	71(1)	6.1(5)	Yang et al. (1998)
Cummingtonite $C2/m$	78(3)	4	Yang et al. (1998)
Grunerite	63(1)	4	Zhang et al. (1992)
Grunerite	50(1)	13(1)	Zhang et al. (1992)
Grunerite-Cummingtonite s.s.	65.4(1.9)	7.0(4)	Boffa Ballaran et al. (2000)
Kaersutite FR12 (oxo)	94(1)	6.3(4)	present work
Kaersutite FR12 (oxo)	100.5(8)	4	present work
Kaersutite DL5	91(2)	6.2(4)	present work
Kaersutite DL5	96.8(7)	4	present work

the bulk moduli increase from 89 to 97 GPa and 101 GPa upon increasing the oxo-component from 0 to nearly 2 apfu. Therefore, it can be concluded that an increasing oxo-component content enlarges the stability of calcic amphiboles toward higher *P*.

Finally, thermodynamic modeling involving amphiboles has to take into account the oxo-component, which determines the density of the phase, the content of water released at the amphibole breakdown, and the phase stability.

ACKNOWLEDGMENTS

The amphibole samples come from the personal collection of Howard Wilshire, who is greatly thanked. Editor Martin Kunz, Associate Editor Darby Dyar, R.K. Popp, and an anonymous referee are gratefully acknowledged for their careful reviews and comments.

REFERENCES CITED

- Allan, D.R., Miletich, R., and Angel, R.J. (1996) A diamond-anvil cell for single-crystal X-ray diffraction studies to pressures in excess of 10 GPa. *Review of Scientific Instruments*, 67, 840–842.
- Alonso-Perez, R., Muntener, O., and Ulmer, P. (2009) Igneous garnet and amphibole fractionation in the roots of island arcs: experimental constraints on andesitic liquids. *Contribution to Mineralogy and Petrology*, 157, 541–558.
- Angel, R.J. (2000) Equation of State. In R.M. Hazen and R.T. Downs, Eds., *High-Temperature and High-Pressure Crystal Chemistry*, 41, p. 35–59. Reviews in Mineralogy and Geochemistry, Mineralogical Society of America and Geochemical Society, Chantilly, Virginia.
- (2004a) Absorb V6.1. Program for absorption. Crystallography Laboratory, Department of Geological Sciences, Virginia Tech, Blacksburg, Virginia.
- (2004b) EOS-FIT V6.1. Computer program. Crystallography Laboratory, Department of Geological Sciences, Virginia Tech, Blacksburg, Virginia.
- Boffa Ballaran, T., Angel, R.J., and Carpenter, M.A. (2000) High-pressure transformation behaviour of the cummingtonite-grunerite solid solution. *European Journal of Mineralogy*, 12, 1195–1213.
- Budzianowski, A. and Katrusiak, A. (2004) High-pressure crystallographic experiments with a CCD-detector. In A. Katrusiak and P. McMillan, Eds., *High-pressure crystallography*, p. 101–112. Kluwer, The Netherlands.
- Cámara, F., Oberti, R., Lezzi, G., and Della Ventura, G. (2003) The $P_{2/m}-C_{2/m}$ phase transition in synthetic amphibole $\text{NaNaMgMg}_5\text{Si}_8\text{O}_{22}(\text{OH})_2$: Thermodynamic and crystal-chemical evaluation. *Physics and Chemistry of Minerals*, 30, 570–581.
- Cameron, M., Sueno, S., Papike, J.J., and Prewitt, C.T. (1983) High-temperature crystal chemistry of K and Na fluor-rich richterites. *American Mineralogist*, 68, 924–943.
- Comodi, P., Mellini, M., Ungaretti, L., and Zanazzi, P.F. (1991) Compressibility and high pressure structure refinement of tremolite, pargasite, and glaucophane. *European Journal of Mineralogy*, 3, 485–499.
- Dyar, M.D., Mackwell, S.J., McGuire, A.V., Cross, L.R., and Robertson, J.D. (1993) Crystal chemistry of Fe^{3+} and H^+ in mantle kaersutite: Implications for mantle metasomatism. *American Mineralogist*, 78, 968–979.
- Forneris, J.F. and Holloway, J.R. (2003) Phase equilibria in subducting basaltic crust: Implications for H_2O release from the slab. *Earth and Planetary Science Letters*, 214, 187–201.
- Fumagalli, P. and Poli, S. (2005) Experimentally determined phase relations in hydrous peridotites to 6.5 GPa and their consequences on the dynamics of subduction zones. *Journal of Petrology*, 46, 555–578.
- Halliday, A.N., Lee, D.C., Tommasini, S., Davies, G.R., Paslick, C.R., Fitton, J.G., and James, D.E. (1995) Incompatible trace elements in OIB and MORB and source enrichment in the sub-oceanic mantle. *Earth and Planetary Science Letters*, 131, 379–395.
- Hauri, E.H., Gaetani, G.A., and Green, T.H. (2006) Partitioning of water during melting of the Earth's upper mantle at H_2O -undersaturated conditions. *Earth and Planetary Science Letters*, 248, 715–734.
- Hawthorne, F.C. and Oberti, R. (2007a) Classification of amphiboles. In F.C. Hawthorne, R. Oberti, G. Della Ventura, and A. Mottana, Eds., *Amphiboles: Crystal chemistry, occurrence, and health issues*, 67, p. 55–88. Reviews in Mineralogy and Geochemistry, Mineralogical Society of America and Geochemical Society, Chantilly, Virginia.
- (2007b) Amphiboles: Crystal chemistry. In F.C. Hawthorne, R. Oberti, G. Della Ventura, and A. Mottana, Eds., *Amphiboles: Crystal chemistry, occurrence, and health issues*, 67, p. 1–54. Reviews in Mineralogy and Geochemistry, Mineralogical Society of America and Geochemical Society, Chantilly, Virginia.
- Hawthorne, F.C., Oberti, R., Della Ventura, G., and Mottana, A. (2007) Amphiboles: Crystal chemistry, occurrence, and health issues, 67, p. 1–545. Reviews in Mineralogy and Geochemistry, Mineralogical Society of America and Geochemical Society, Chantilly, Virginia.
- Ionov, D.A. and Hofmann, A.W. (1995) Nb-Ta-rich mantle amphiboles and micas: Implications for subduction-related metasomatic trace element fractionations. *Earth and Planetary Science Letters*, 131, 341–356.
- Ionov, D.A., Bodinier, J.-L., Mukasa, S.B., and Zanetti, A. (2002) Mechanisms and sources of mantle metasomatism: Major and trace element compositions of peridotite xenoliths from Spitsbergen in the context of numerical modeling. *Journal of Petrology*, 43, 2219–2259.
- Irving, A.J. and Green, D.H. (2008) Phase relationships of hydrous alkalic magmas at high pressures: Production of nepheline hawaiitic to mugearitic liquids by amphibole-dominated fractional crystallization within the lithospheric mantle. *Journal of Petrology*, 49, 741–756.
- Jeanloz, R. and Hazen, R.M. (1991) Finite-strain analysis of relative compressibilities. Application to the high-pressure wadsleyite phase as an illustration. *American Mineralogist*, 76, 1765–1768.
- Jenkins, D.M. and Corona, J.C. (2006) Molar volume and thermal expansion of glaucophane. *Physics and Chemistry of Minerals*, 33, 356–362.
- King, H.E. and Finger, L.W. (1979) Diffracted beam crystal centering and its application to high-pressure crystallography. *Journal of Applied Crystallography*, 12, 374–378.
- Leake, B.E., Woolley, A.R., Arps, C.E.S., Birch, W.D., Gilbert, M.C., Grice, J.D., Hawthorne, F.C., Kato, A., Kish, H.J., Krivovichev, V.G., Linthout, K., Laird, J., Mandarin, J.A., Maresch, W.V., Nickel, E.H., Rock, N.M.S., Schumaker, J.C., Smith, D.C., Stephenson, N.C.N., Ungaretti, L., Whittaker, E.J.W., and Guo, Y. (1997) Nomenclature of amphiboles: Report of the subcommittee on amphiboles of the International Mineralogical Association, Commission on New Minerals and Mineral Names. *American Mineralogist*, 82, 1019–1037.
- Leake, B.E., Woolley, A.R., Birch, W.D., Burke, E.A.J., Ferraris, G., Grice, J.D., Hawthorne, F.C., Kish, H.J., Krivovichev, V.G., Schumaker, J.C., Stephenson, N.C.N., and Whittaker, E.J.W. (2003) Nomenclature of amphiboles: additions and revisions to the International Mineralogical Association's amphibole nomenclature. *Canadian Mineralogist*, 41, 1355–1370.
- Mao, H.K., Xu, J., and Bell, P.M. (1986) Calibration of the ruby pressure gauge to 800 kbar under quasi-hydrostatic conditions. *Journal of Geophysical Research*, 91, 4673–4676.
- Miletich, R., Allan, D.R., and Kuhs, W.F. (2000) High-pressure single-crystal techniques. In R.M. Hazen and R.T. Downs, Eds., *High-Temperature and High-Pressure Crystal Chemistry*, 41, p. 445–519. Reviews in Mineralogy and Geochemistry, Mineralogical Society of America and Geochemical Society, Chantilly, Virginia.
- Niida, K. and Green, D.H. (1999) Stability and chemical composition of pargasitic amphibole in MORB pyrolyte under upper mantle conditions. *Contributions to Mineralogy and Petrology*, 135, 18–40.
- Oberti, R., Della Ventura, G., and Cámara, F. (2007a) New amphiboles compositions: Natural and synthetic. In F.C. Hawthorne, R. Oberti, G. Della Ventura, and A. Mottana, Eds., *Amphiboles: Crystal chemistry, occurrence, and health issues*, 67, p. 89–113. Reviews in Mineralogy and Geochemistry, Mineralogical Society of America and Geochemical Society, Chantilly, Virginia.
- Oberti, R., Hawthorne, F.C., Cannillo, E., and Cámara, F. (2007b) Long-range order in amphiboles. In F.C. Hawthorne, R. Oberti, G. Della Ventura, and A. Mottana, Eds., *Amphiboles: Crystal chemistry, occurrence and health issues*, 67, p. 125–171. Reviews in Mineralogy and Geochemistry, Mineralogical Society of America and Geochemical Society, Chantilly, Virginia.
- Oberti, R., Boiocchi, M., Ball, N.A., and Hawthorne, F.C. (2009a) Fluoro-sodic-ferropedrite, $\text{NaLi}_2(\text{Fe}^{2+}\text{Al}_2\text{Li})\text{Si}_5\text{O}_{22}\text{F}_2$, a new mineral of the amphibole group from the Sutlug River, Tuva Republic, Russia: description and crystal structure. *Mineralogical Magazine*, 73, 487–494.
- Oberti, R., Zema, M., Boiocchi, M., Tarantino, S., and Zanetti, A. (2009b) Thermal expansion and dehydrogenation processes in kaersutites: II—models at the atomic scale. VII Forum Italiano di Scienze della Terra, Rimini, September 9–11, Italy.
- Oberti, R., Zema, M., Tarantino, S., and Boiocchi, M. (2009c) Thermal expansivity and dehydrogenation in amphiboles. 25th European Crystallographic Meeting, ECM25, Istanbul 2009. *Acta Crystallographica*, A65, s176.
- Ohashi, Y. (1982) A program to calculate the strain tensor from two sets of unit-cell parameters. In R.M. Hazen and L.W. Finger, Eds., *Comparative Crystal Chemistry: Temperature, pressure, composition and the variation of crystal structure*, p. 92–102. Wiley, London.
- Poli, S. and Schmidt, M.W. (1995) Water transport and release in subduction zones: Experimental constraints on basaltic and andesitic systems. *Journal of Geophysical Research*, 100, 22299–22314.
- Robinson, K., Gibbs, G.V., and Ribbe, P.H. (1971) Quadratic elongation, a quantitative measure of distortion in coordination polyhedra. *Science*, 172, 191–193.
- Sheldrick, G.M. (1996) SADABS. Program for empirical absorption correction of area detector data. Institut für Anorganische Chemie, University of Göttingen, Germany
- (1997) SHELX-97. Programs for crystal structure determination and refine-

- ment. Institut für Anorganische Chemie, University of Göttingen, Germany.
- Smyth, J.R., Jacobsen, S.D., and Hazen, R.M. (2000) Comparative crystal chemistry of orthosilicate minerals. In R.M. Hazen and R.T. Downs, Eds., *High-Temperature and High-Pressure Crystal Chemistry*, 41, p. 187–209. Reviews in Mineralogy and Geochemistry, Mineralogical Society of America and Geochemical Society, Chantilly, Virginia.
- Sueno, S., Cameron, M., Papike, J.J., and Prewitt, C.T. (1973) High-temperature crystal chemistry of tremolite. *American Mineralogist*, 58, 649–664.
- Tiepolo, M., Zanetti, A., and Oberti, R. (1999) Detection, crystal-chemical mechanisms and petrological implications of $^{16}\text{Ti}^{4+}$ partitioning in pargasite and kaersutite. *European Journal of Mineralogy*, 11, 345–354.
- Tiepolo, M., Oberti, R., Zanetti, A., Vannucci, R., and Foley, S.F. (2007) Trace-element partitioning between amphibole and silicate melts. In F.C. Hawthorne, R. Oberti, G. Della Ventura, and A. Mottana, Eds., *Amphiboles: Crystal chemistry, occurrence, and health issues*, 67, p. 417–451. Reviews in Mineralogy and Geochemistry, Mineralogical Society of America and Geochemical Society, Chantilly, Virginia.
- Tribaudino, M., Bruno, M., Iezzi, G., Della Ventura, G., and Margiolaki, I. (2008) The thermal behavior of richterite. *American Mineralogist*, 93, 1659–1665.
- Vannucci, R., Piccardo, G.B., Rivalenti, G., Zanetti, A., Rampone, E., Ottolini, L., Oberti, R., Mazzucchelli, M., and Bottazzi, P. (1995) Origin of LREE-depleted amphiboles in the subcontinental mantle. *Geochimica et Cosmochimica Acta*, 59, 1763–1771.
- Wallace, M.E. and Green, D.H. (1991) The effect of bulk rock composition on the stability of amphibole in the upper mantle: Implication for solidus positions and mantle metasomatism. *Mineralogy and Petrology*, 44, 1–19.
- Welch, M.D., Cámara, F., Della Ventura, G., and Iezzi, G. (2007) Non-ambient in situ studies of amphiboles. In F.C. Hawthorne, R. Oberti, G. Della Ventura, and A. Mottana, Eds., *Amphiboles: Crystal chemistry, occurrence, and health issues*, 67, p. 223–260. Reviews in Mineralogy and Geochemistry, Mineralogical Society of America and Geochemical Society, Chantilly, Virginia.
- Wilson, A.J.C. and Prince, E. (1999) *International Tables for X-ray Crystallography, Volume C: Mathematical, physical and chemical tables* (2nd ed.). Kluwer, The Netherlands.
- Yang, H., Hazen, R.M., Prewitt, C.T., Finger, L.W., Lu, R., and Hemley, R.J. (1998) High-pressure single-crystal X-ray diffraction and infrared spectroscopic studies of the $C2/m-P2_1/m$ phase transition in cummingtonite. *American Mineralogist*, 83, 288–299.
- Zanetti, A., Oberti, R., Bottazzi, P., and Vannucci, R. (1997) Fe^{3+} contents in partially-dehydrogenated high-T amphiboles by combining SREF, EMP, and SIMS analyses: An insight into intensive parameters of upper mantle. *EUG 9*, Strasbourg, France, 23–27 Marzo, Terra Nova, 9, 437.
- Zanetti, A., Pedrazzi, G., and Oberti, R. (2000) Accurate determination of Fe^{2+} and Fe^{3+} site-partitioning in pargasite and kaersutite: An integrated SREF, EMP, SIMS, and Mössbauer study. *Plinius*, 24, 220–221.
- Zema, M., Oberti, R., Boiocchi, M., and Tarantino, S. (2009) Thermal expansion and dehydrogenation processes in kaersutites: I-effects on unit-cell parameters. VII Forum Italiano di Scienze della Terra, Rimini, September 9–11, Italy.
- Zhang, L., Ahsbahs, H., Kutoglu, A., and Hafner, S.S. (1992) Compressibility of grunerite. *American Mineralogist*, 77, 480–483.

MANUSCRIPT RECEIVED OCTOBER 14, 2009

MANUSCRIPT ACCEPTED FEBRUARY 16, 2010

MANUSCRIPT HANDLED BY M. DARBY DYAR